Fractal Dimensions and Mixing Structures of Soot Particles during Atmospheric Processing

Wang, Yuanyuan; Liu, Fengshan; He, Cenlin; Bi, Lei; Cheng, Tianhai; Wang, Zhili; Zhang, Hua; Zhang, Xiaoye; Shi, Zongbo; Li, Weijun

DOI:
10.1021/acs.estlett.7b00418

Document Version
Peer reviewed version

Citation for published version (Harvard):
Wang, Y, Liu, F, He, C, Bi, L, Cheng, T, Wang, Z, Zhang, H, Zhang, X, Shi, Z & Li, W 2017, 'Fractal Dimensions and Mixing Structures of Soot Particles during Atmospheric Processing', *Environmental Science and Technology Letters*, vol. 4, no. 11, pp. 487-493. https://doi.org/10.1021/acs.estlett.7b00418

Fractal Dimensions and Mixing Structures of Soot Particles during Atmospheric Processing

Yuanyuan Wang[1,2], Fengshan Liu[3], Cenlin He[4], Lei Bi[2], Tianhai Cheng[5], Zhili Wang[6], Hua Zhang[7,8], Xiaoye Zhang[6], Zongbo Shi[9], Weijun Li[*2]

[1]Environment Research Institute, Shandong University, Jinan, Shandong 250100, China

[2]Department of Atmospheric Sciences, School of Earth Sciences, Zhejiang University, Hangzhou, 310027, China

[3]Measurement Science and Standards, National Research Council, Ottawa, Ontario K1A 0R6, Canada

[4]Department of Atmospheric and Oceanic Sciences and Joint Institute for Earth System Science and Engineering, University of California, Los Angeles, CA90095, USA

[5]State Key Laboratory of Remote Sensing Science, Institute of Remote Sensing and Digital Earth, Chinese Academy of Sciences, Beijing, 100101, China

[6]Chinese Academy of Meteorological Sciences, Beijing 100081, China

[7]Collaborative Innovation Center on Forecast and Evaluation of Meteorological Disasters, Nanjing University of Information Science & Technology, Nanjing 210044, China

[8]Laboratory for Climate Studies, National Climate Center, China Meteorological Administration, Beijing 100081, China

[9]School of Geography, Earth and Environmental Sciences, University of Birmingham, Birmingham B15 2TT, U.K

* Corresponding author: liweijun@zju.edu.cn

+86-57187952453

Abstract

Soot particles strongly absorb sunlight and hence act as a short-lived warming agent. Atmospheric aging of soot particles changes their morphology and mixing state and consequently alter their optical properties. Here we collected soot particles at tunnel, urban, mountaintop, and background sites in Northern China and analyzed their mixing structures and morphology using transmission electron microscopy. Soot particles were further classified into three types: bare-like, partly coated, and embedded. Bare-like soot particles were dominant at the tunnel site, while most soot particles were partly coated or embedded type at other sites. Fractal dimensions (D_f) of different types of soot particles ranged from 1.80 to 2.16 and were ordered as: bare-like < partly coated < embedded. Moreover, their average D_f changed from 1.8 to 2.0 from the tunnel to the background site. We conclude that the D_f can characterize the shape of soot aggregates reasonably well and its variation reflects soot aging processes. Compared with the reported D_f of soot particles, we found that D_f = 1.8 used in previous optical models primarily represents freshly emitted soot aggregates, rather than the ambient ones.

1 Introduction

Soot particles, also known as black carbon (BC) or elemental carbon (EC), are fractal-like aggregates produced from the incomplete combustion of biomass and fossil fuels. Soot particles strongly absorb sunlight and heat the air, altering the radiative forcing of the atmosphere and affecting global and regional climate.[1-4] During transport and aging, fresh soot particles mix with organic and inorganic aerosols, changing their morphology and compactness, which leads to changes of their optical properties and radiative forcing.[5, 6] *Jacobson*[7] proposed that the sulfate coating on soot particles can enhance optical absorption by ~2 through treating the mixture of soot and sulfate as a core-shell model. However, *Cappa et al.*[8] observed that the absorption enhancement of aged soot particles in Sacramento was 6% on average at 532 nm by in-situ measurements. Different conclusions about the optical absorption of soot particles should be attributed to their complicated shapes and various mixing states in the atmosphere.[9, 10] Due to the lack of quantification on the variation of shapes and mixing structures of soot particles, the debate on optical properties of soot particles still continues.

Some experimental methods such as combination of single-particle soot photometer (SP2), three-wavelength photoacoustic soot spectrometer (PASS-3), and Aerodyne soot particle-aerosol mass spectrometer (SP-AMS) were used to well characterize physicochemical properties of soot and measured their optical properties.[11-14] However, these measurements could not provide accurate morphology of soot aggregates for the modeling study. Many numerical optical models such as the Rayleigh-Debye-Gans (RDG) approximation[15], T-Matrix[16, 17], and Discrete Dipole Approximation (DDA)[18] can be used to calculate the optical properties of soot aggregates.[10, 19-21] Except RDG, other numerical models require the morphology of soot aggregates, which can be generated numerically using fractal dimension (D_f). Among the available algorithms to generate fractal aggregates, the tunable method[22] is preferred due to its capability of generating aggregates of a prescribed D_f, which is the most important morphological parameter of fractal aggregates. *Adachi et al.*[23] used electron tomography in transmission electron microscopy (TEM) to calculate the D_f of individual soot particles. The method requires a sophisticated system of TEM coupled with tomography, which is not commonly available. *Xiong and Friedlander*[24] calculated the D_f of individual soot particles by drawing circles around the primary particles and then determining the size and position of the primary particles in the TEM image using scaling laws.[25, 26] The method is inefficient in obtaining the D_f of hundreds of soot particles, because it requires 10-30 minutes for each soot aggregate. Later, an approach for image characterization of soot aggregates was proposed by *Brasil et al.*[27] and *Oh and Sorensen*.[28] The method can conveniently derive various parameters of individual soot particles in the scaling law and obtain a D_f to represent their ensemble morphology. Recently, *China et al.*[29] successfully used this method to calculate D_f of soot particles freshly emitted by wildfire. However, there are only quite few available reports about the D_f of ambient soot particles, whose D_f values are very important to understand their optical properties in different environments.

In this study, we report a detailed analysis of a large number of soot particles collected at tunnel, urban, mountaintop, and background sites in polluted air in the North China Plain (NCP). At each site, soot particles are classified into three types based on their mixing states and morphology and then their corresponding D_f values are calculated and compared systematically for the first time. We use a method combining TEM analysis and numerical calculation to obtain a D_f to represent the ensemble morphology of soot aggregates. At last, we discuss their morphological and mixing properties and the implication of these properties on aging.

2 Materials and Methods

2.1 Aerosol Sampling

The NCP was covered by the regional haze layer during the sampling period, so we defined our samples from the continental polluted air. Aerosol samples were collected at four sampling sites in NCP: a tunnel site, an urban site, a mountaintop site, and a background site (Figure S1), where the relative humidities (RHs) were at about 52%, 16%, 64%, and 56%, respectively. The RHs at the four sampling sites were lower than 65% during the sampling period, indicating that the hazes were mainly dry. The Kaiyuan tunnel site is a busy highway that enters Jinan City. The urban site in Jinan City is a typical downtown site with strong vehicle and residential emissions. The Mountain Tai (at 1534 m above sea level) is the highest mountain in NCP. The aerosol particles collected at the mountaintop site reflect regional transport of aerosol particles in NCP.[30] The background Changdao Island in the Bohai Sea is a downwind site of Shandong province and the Jing-Jin-Ji area (i.e., Beijing, Tianjin, and Hebei province) during winter (Figure S1). Aerosol samples were simultaneously collected at the urban, mountaintop, and background sites during 13-23 December 2014. At the tunnel site, aerosol samples were collected on 8 November 2016. A total of 779 soot particles from 31 samples were analyzed to determine their size and elemental composition using TEM/EDS. We note that the distribution of aerosol particles on TEM grids was not uniform. Therefore, we chose three to four areas from the center and periphery of each grid to ensure that the analyzed particles were representative. Once the internally mixed soot particles are under the strong electron beam (Figure S2), they can easily damage the sulfates and nitrates but do not change morphology of soot aggregates. This microscopic analysis is explained in the Supporting Information.

2.2 Morphology Analysis of Soot Particles

Fractal dimension of soot particles can be characterized using the scaling law[25]:

$$N = k_g \left(\frac{2R_g}{d_p} \right)^{D_f} \tag{1}$$

where N is the total number of monomers in each aggregate, R_g is the radius of gyration of the soot aggregate, d_p is the monomer diameter, k_g is the fractal prefactor, and D_f is the mass fractal dimension. Note that the D_f in this study is the mass fractal dimension of soot aggregates that excludes the coating. In this study, the D_f and k_g are estimated from a power law fit of a scatter plot of N vs the values of $2R_g/d_p$.

N can also be scaled with the aggregate projected area in the following power-law relationship:

$$N = k_a \left(\frac{A_a}{A_p} \right)^{\alpha} \quad (2)$$

$$\delta = \frac{2a}{l} \quad (3)$$

where A_a is the projected area of the soot aggregate, A_p is the mean projected area of the monomer, k_a is a constant, and α is an empirical projected area exponent. The exact values of k_a and α depend on the overlap parameter (δ),[28] which can be calculated using equation (3) with a being the monomer radius and l the lattice spacing in TEM images. The number of monomers N can then be calculated using equation (2).[28]

The parameters d_p and R_g are also required to determine D_f. While d_p can be obtained directly from analysis of TEM images, estimation of the actual radius of gyration (R_g) is complicated. Here we used the following simple correlation

$$L_{\max} / (2R_g) = 1.50 \pm 0.05 \quad (4)$$

to calculate R_g,[27] where L_{max} is the maximum length of the soot aggregate obtained from TEM images.

3 Results and Discussion

3.1 Morphology and Mixing State of Soot Particles

Fresh soot particles are normally chain-like aggregates. Once soot particles mix with other aerosol components in the air, the aging process can rearrange the structure of the inner soot aggregates.[31] Based on their morphology and the visual estimation of coating on soot particles in TEM images, we classified them into three types: bare-like, partly coated, and embedded. Bare-like soot particles in TEM images display clear monomers without any visible coating on their surface (Figure 1a-1/1b-1/1c-1). Partly coated soot particles mean that individual soot particles are partly coated by other aerosol components (Figure 1a-2/1b-2/1c-2). Embedded soot particles refer to individual soot particles that are heavily coated or are entirely embedded within other aerosol components (Figure 1a-3/1b-3/1c-3). Figure 1 shows the three types of soot particles collected at the urban, mountaintop, and background sampling sites. Bare-like soot particles are dominant in the tunnel samples, because vehicles emit large amounts of fresh soot particles (Figure S3). Similar results have been found near freeways.[32] Based on their different mixing structures, embedded soot particles are normally considered as more aged than the partly coated soot particles.[33] We also calculated the area ratios of coating/soot core for internally mixed soot particles. Figure S4 shows partly coated soot particles mostly have ratios smaller than one, indicating smaller coatings. In contrast, embedded soot particles have lager ratios, some of which are more than 20 times larger. These results are consistent with our classification.

Figure 2 shows the fractions of three types of soot particles in different atmospheric environments. The result shows that the bare-like soot particles accounted for 64% of all particles in tunnel air but only 1~25% in urban polluted air (Figure 2). *Wang et al.*[34] also found a fairly low fraction (31.2%) of externally mixed soot particles in urban Xi'an City of China through a single-particle soot photometer (SP2). As a result, the polluted air likely accelerated the transformation from bare-like into partly coated or embedded soot particles.[33] It should be noted that bare-like soot particles accounted for 25% at the urban site and 21% at the background site, but embedded soot particles significantly increased from 12% to 39% (Figure 2). These results indicate that the polluted air masses from the Jing-Jin-Ji area and Shandong province (Figure S1) brought a large number of aged soot particles into the downwind background air. In addition, the fraction of embedded soot particles at the mountaintop site is largest at 55% and bare-like soot is lowest at 1% among the three sampling sites. *China et al.*[35] found that most soot particles from North America became internally mixed at the summit caldera of the Pico Volcano. Therefore, soot particles that are emitted mostly at ground level but transported into the upper atmospheric layers could undergo intense aging processes during their transports. The RH is a critical factor to enhance heterogeneous reactions of acidic gases on particle surface because secondary aerosols can deliquesce at about 60-80%

RH and form liquid phases.[36] During the sampling period, there was higher RH around 64% in the upper air than the 16-55% on the ground. Indeed, many embedded soot particles on the mountaintop left a water rim around sulfate coating after drying on the substrate (Figure 1b-3), which indicates that secondary aerosol components existed as the liquid phase in the air.[33] We conclude that soot particles likely underwent more complicated ageing processes due to the higher RH of the upper layers than at the polluted ground sites.

3.2 Quantifying the Shapes of Soot Particles

It is widely acknowledged that D_f of soot particles reflects their combustion conditions and aging processes.[23] Compact soot particles often have larger D_f than lacy aggregates.[37] Here we calculated the D_f of soot particles collected at the four sampling sites (Figure 3). D_f of bare-like soot particles at different sampling sites was very close, at ~1.82 (Figure 3a, 3b, 3d). Bare-like soot particles have the lowest D_f followed by partly coated and embedded soot particles (Figure 3), suggesting that bare-like soot particles were more lacy compared to the partly coated and embedded types. D_f of partly coated soot particles tends to be ~1.87, smaller than the 1.90~2.16 of embedded soot particles (Figure 3). Similarly, *China et al.*[29] found the same properties (i.e., bare-like < partly coated < embedded) of D_f of the three types of soot particles emitted by wildfires. *Peng et al.*[38] also found that the morphology of soot particles was modified heavily during aging processes. For the background soot particles, D_f ranges between 1.83 and 2.16, with a medium of 2.00 (Figure 3d). In contrast, D_f of the urban soot particles has lower values, between 1.83 and 1.90. We multiplied the number fraction of each type of soot by their corresponding D_f to calculate the statistical weighting of D_f. The statistical weighting of D_f values of the urban, mountaintop, and background site are 1.87, 1.90, and 1.97, respectively, which have an average value of 1.91.

The convexity (*CV*), roundness (*RN*), and D_f of the three types of soot particles at the four sampling sites are listed in Table S1. The *CV* and *RN* distributions of the three types of soot particle at the same sampling site (Figure S5) clearly prove their

D_f changes (Figure 3). The *CV* and *RN* of bare-like soot particles are smallest followed by those of partly coated and embedded soot particles at the four sampling sites. We therefore conclude that larger *CV* and larger *RN* represent more compactness for aged soot particles, consistent with the study of *China et al*.[29]

We found that D_f of fresh soot particles retained a consistent value (~1.82) at different sampling sites in the polluted air (Figure 3), although fresh soot particles display slightly different D_f due to their different sources and combustion conditions.[39] Many researchers obtained D_f of soot particles of the primary sources, such as D_f from biomass burning at 1.67-1.83[40], D_f from vehicle emissions 1.52-1.94[32], and D_f from diesel at 1.6-1.9[41]. D_f of soot particles becomes larger when soot aggregates are coated by other components during atmospheric processes.[42] This indicates that soot particles likely collapse during the coating processes. In addition, the wide range of D_f of soot particles in the background air is somewhat expected because they originate from multiple sources, such as industries, residential heating, and transportation,[30] and have undergone different atmospheric aging durations and processes.[23] In addition, the D_f of embedded soot particles at 1.90~2.16 in this study are much lower than 2.3~2.6 reported by some previous studies.[21, 23, 43] *Adachi et al.*[21, 23] used cube-counting method to calculate D_f of soot particles. In most cases the images of fractal aggregates cannot be decomposed at all scales into an integer number of square boxes using this method,[44] which may lead to a larger D_f. In the study by *Bambha at al.*,[43] the smaller monomer diameter may cause lesser structural compaction.[45] Besides, the coating material condensed at a low humidity often causes no restructuring, whereas the coating liquefies at a higher humidity and restructuring occurs promptly.[46] In a word, these differences could be attributed to data processing methods, aging environments, and soot aggregate properties.

Using the scaling law method, the previous studies reported D_f at 1.52~1.94 for soot particles at road side[32] and D_f > 2 for soot particles at a remote marine troposphere site.[35] Here we systematically studied D_f of ambient soot particles collected at three representative polluted sites. These data are crucial to assess the accurate shape of soot particles in the dry continental air.

4 Atmospheric Implications

Previous studies reported that the fractal dimensions (D_f) of fresh soot particles from vehicles, biomass, diesel, and wildfire emissions are around 1.73[32], 1.75[40], 1.75[41], and 1.89[29], respectively, which are close to 1.80~1.83 (D_f) of the bare-like soot particles obtained in this study (Figure 3). The reason is that fresh soot particles are generally formed via a cluster-dilute aggregation mechanism in a small-scale burning regime.[39, 47] These fresh soot particles are hydrophobic before being affected by secondary aerosols and condensable vapors in the atmosphere.[48] Therefore, fresh soot particles can hardly collapse and their structures remain largely unchanged. In contrast, once soot particles interact with secondary organic and inorganic aerosols and water vapor during long-range transport, they became more compact as evidenced by the larger D_f in mountaintop and background air (Figure 3). TEM images further show that the morphology of soot particles not only became more compact from vehicular emission to background air (Figure 1), but also possibly underwent reconstruction under the influence of water vapor.[5, 49] Therefore, these hygroscopic secondary aerosols heavily caused morphological changes of soot particles in the atmosphere.

In this study, the D_f of soot particles were found to vary from 1.80 to 2.16 (Figure 3d) for different mixing structures, which indicate that the mixing structure of soot particles can represent their aging degree.[31, 33] At present, many studies set D_f as ~1.8 to simulate the complex structure of soot particles and to further calculate their optical properties.[10, 50-52] However, some studies have suggested that the highly compact soot particles have substantially different optical properties from the lacy ones.[20, 53, 54] In particular, the mass-specific scattering cross sections (MSC) of soot particles follow the order: $D_f = 2.1 > D_f = 1.78 > D_f = 1.4$.[20] Therefore, it is essential to select suitable D_f values to construct accurate optical models of soot particles. Our results show that the statistical weighting of D_f of soot samples collected at the urban, mountaintop, and background site has an average value at 1.91, suggesting that D_f = 1.91 could be more representative for ambient soot particles in continental polluted air. In particular, D_f = 1.91 can well represent soot particles in dry (RH<65%), winter polluted air in North China. Further studies are required to quantify the D_f of soot particles in different atmospheric environments, such as in humid， troposphere, and strongly photochemical air, because they all can accelerate soot aging in the atmosphere.[5, 34]

Acknowledgments

We thank Peter Hyde for his editorial comments. This work was funded by the National Natural Science Foundation of China (41622504 and 41575116) and the Hundred Talents Program in Zhejiang University. ZS is funded by Natural Environment Research Council (NE/N007190/1).

Associated Contents

Supporting Information Available: specific microscopic analysis, related geometric parameters of soot particles, and some supplementary tables and figures.

References

1. Bond, T. C.; Streets, D. G.; Yarber, K. F.; Nelson, S. M.; Woo, J. H.; Klimont, Z., A technology‐based global inventory of black and organic carbon emissions from combustion. *Journal of Geophysical Research Atmospheres* **2004,** *109*, 1149-1165.
2. Ramanathan, V.; Carmichael, G., Global and regional climate changes due to black carbon. *Nature Geoscience* **2008,** *1*, 221-227.
3. Bond, T. C.; Doherty, S. J.; Fahey, D. W.; Forster, P. M.; Berntsen, T.; Deangelo, B. J.; Flanner, M. G.; Ghan, S.; Kärcher, B.; Koch, D., Bounding the role of black carbon in the climate system: A scientific assessment. *Journal of Geophysical Research: Atmospheres* **2013,** *118*, 5380-5552.
4. Adler, G.; Riziq, A. A.; Erlick, C.; Rudich, Y., Effect of intrinsic organic carbon on the optical properties of fresh diesel soot. *Proceedings of the National Academy of Sciences* **2010,** *107*, 6699-6704.
5. Zhang, R.; Khalizov, A. F.; Pagels, J.; Zhang, D.; Xue, H.; McMurry, P. H., Variability in morphology, hygroscopicity, and optical properties of soot aerosols during atmospheric processing. *Proceedings of the National Academy of Sciences* **2008,** *105*, 10291-10296.
6. Zhou, C.; Zhang, H.; Zhao, S.; Li, J., Simulated effects of internal mixing of anthropogenic aerosols on the aerosol–radiation interaction and global temperature. *International Journal of Climatology* **2017**, 972-986.
7. Jacobson, M. Z., Strong radiative heating due to the mixing state of black carbon in atmospheric aerosols. *Letters to nature* **2001,** *409*, 695-697.
8. Cappa, C. D.; Onasch, T. B.; Massoli, P.; Worsnop, D. R.; Bates, T. S.; Cross, E. S.; Davidovits, P.; Hakala, J.; Hayden, K. L.; Jobson, B. T.; Kolesar, K. R.; Lack, D. A.; Lerner, B. M.; Li, S.-M.; Mellon, D.; Nuaaman, I.; Olfert, J. S.; Petäjä, T.; Quinn, P. K.; Song, C.; Subramanian, R.; Williams, E. J.; Zaveri, R. A., Radiative Absorption Enhancements Due to the Mixing State of Atmospheric Black Carbon. *Science* **2012,** *337*, 1078-1081.
9. Liu, D.; Whitehead, J.; Alfarra, M. R.; Reyes-Villegas, E.; Spracklen, D. V.; Reddington, C. L.; Kong, S.; Williams, P. I.; Ting, Y.-C.; Haslett, S.; Taylor, J. W.; Flynn, M. J.; Morgan, W. T.; McFiggans, G.; Coe, H.; Allan, J. D., Black-carbon absorption enhancement in the atmosphere determined by particle mixing state. *Nature Geosci* **2017,** *10*, 184-188.
10. Scarnato, B. V.; Vahidinia, S.; Richard, D. T.; Kirchstetter, T. W., Effects of internal mixing and aggregate morphology on optical properties of black carbon using a discrete dipole approximation model. *Atmospheric Chemistry and Physics* **2013,** *13*, 5089-5101.
11. Wang, J.; Ge, X.; Chen, Y.; Shen, Y.; Zhang, Q.; Sun, Y.; Xu, J.; Ge, S.; Yu, H.; Chen, M., Highly time-resolved urban aerosol characteristics during springtime in Yangtze River Delta, China: insights from soot particle aerosol mass spectrometry. *Atmos. Chem. Phys.* **2016,** *16*, 9109-9127.
12. Lan, Z.-J.; Huang, X.-F.; Yu, K.-Y.; Sun, T.-L.; Zeng, L.-W.; Hu, M., Light absorption of black carbon aerosol and its enhancement by mixing state in an urban atmosphere in South China. *Atmospheric Environment* **2013,** *69*, 118-123.
13. Liu, S.; Aiken, A. C.; Gorkowski, K.; Dubey, M. K.; Cappa, C. D.; Williams, L. R.; Herndon, S. C.; Massoli, P.; Fortner, E. C.; Chhabra, P. S.; Brooks, W. A.; Onasch, T. B.; Jayne, J. T.; Worsnop, D. R.; China, S.; Sharma, N.; Mazzoleni, C.; Xu, L.; Ng, N. L.; Liu, D.; Allan, J. D.; Lee, J. D.; Fleming, Z. L.; Mohr, C.; Zotter, P.; Szidat, S.; Prevot, A. S., Enhanced light absorption by mixed source black and brown carbon particles in UK winter. *Nature communications* **2015,** *6*, 8435, doi:10.1038/ncomms9435.

14. Wang, J.; Onasch, T. B.; Ge, X.; Collier, S.; Zhang, Q.; Sun, Y.; Yu, H.; Chen, M.; Prévôt, A. S. H.; Worsnop, D. R., Observation of Fullerene Soot in Eastern China. *Environmental Science & Technology Letters* **2016,** *3*, 121-126.

15. Farias, T. L.; Köylü, U.; Carvalho, M. G., Range of validity of the Rayleigh-Debye-Gans theory for optics of fractal aggregates. *Applied optics* **1996,** *35*, 6560-6567.

16. Bi, L.; Yang, P.; Kattawar, G. W.; Mishchenko, M. I., Efficient implementation of the invariant imbedding T-matrix method and the separation of variables method applied to large nonspherical inhomogeneous particles. *Journal of Quantitative Spectroscopy and Radiative Transfer* **2013,** *116*, 169-183.

17. Mackowski, D. W.; Mishchenko, M. I., A multiple sphere T-matrix Fortran code for use on parallel computer clusters. *Journal of Quantitative Spectroscopy and Radiative Transfer* **2011,** *112*, 2182-2192.

18. Draine, B. T.; Flatau, P. J., Discrete-Dipole Approximation For Scattering Calculations. *J. Opt. Soc. Am. A* **1994,** *11*, 1491-1499.

19. Liu, C.; Yin, Y.; Hu, F.; Jin, H.; Sorensen, C. M., The Effects of Monomer Size Distribution on the Radiative Properties of Black Carbon Aggregates. *Aerosol Science and Technology* **2015,** *49*, 928-940.

20. Liu, F.; Wong, C.; Snelling, D. R.; Smallwood, G. J., Investigation of Absorption and Scattering Properties of Soot Aggregates of Different Fractal Dimension at 532 nm Using RDG and GMM. *Aerosol Science and Technology* **2013,** *47*, 1393-1405.

21. Adachi, K.; Chung, S. H.; Buseck, P. R., Shapes of soot aerosol particles and implications for their effects on climate. *Journal of Geophysical Research: Atmospheres* **2010,** *115*, 4447-4458.

22. Skorupski, K.; Mroczka, J.; Wriedt, T.; Riefler, N., A fast and accurate implementation of tunable algorithms used for generation of fractal-like aggregate models. *Physica A: Statistical Mechanics and its Applications* **2014,** *404*, 106-117.

23. Adachi, K.; Chung, S. H.; Friedrich, H.; Buseck, P. R., Fractal parameters of individual soot particles determined using electron tomography: Implications for optical properties. *Journal of Geophysical Research: Atmospheres* **2007,** *112*, 2156-2202.

24. Xiong, C.; Friedlander, S. K., Morphological properties of atmospheric aerosol aggregates. *Proceedings of the National Academy of Sciences* **2001,** *98*, 11851-11856.

25. Koeylue, U.; Xing, Y.; Rosner, D. E., Fractal Morphology Analysis of Combustion-Generated Aggregates Using Angular Light Scattering and Electron Microscope Images. *Langmuir* **1995,** *11*, 4848-4854.

26. Forrest, S. R.; T. A. Witten, J., Long-range correlations in smoke-particle aggregates. *Journal of Physics A: Mathematical and General* **1979,** *12*, L109-L117.

27. Brasil, A. M.; Farias, T. L.; Carvalho, M. G., A recipe for image characterization of fractal-like aggregates. *Journal of Aerosol Science* **1999,** *30*, 1379-1389.

28. Oh, C.; Sorensen, C. M., The Effect of Overlap between Monomers on the Determination of Fractal Cluster Morphology. *Journal of Colloid & Interface Science* **1997,** *193*, 17-25.

29. China, S.; Mazzoleni, C.; Gorkowski, K.; Aiken, A. C.; Dubey, M. K., Morphology and mixing state of individual freshly emitted wildfire carbonaceous particles. *Nature communications* **2013,** *4*, 2122, doi: 10.1038/ncomms3122.

30. Chen, S.; Xu, L.; Zhang, Y.; Chen, B.; Wang, X.; Zhang, X.; Zheng, M.; Chen, J.; Wang, W.; Sun, Y.; Fu, P.; Wang, Z.; Li, W., Direct observations of organic aerosols in common wintertime hazes in

North China: insights into direct emissions from Chinese residential stoves. *Atmos. Chem. Phys.* **2017,** *17*, 1259-1270.

31. Riemer, N.; Vogel, H.; Vogel, B., Soot aging time scales in polluted regions during day and night. *Atmos. Chem. Phys.* **2004,** *4*, 1885-1893.

32. China, S.; Salvadori, N.; Mazzoleni, C., Effect of traffic and driving characteristics on morphology of atmospheric soot particles at freeway on-ramps. *Environmental science & technology* **2014,** *48*, 3128-3135.

33. Li, W.; Sun, J.; Xu, L.; Shi, Z.; Riemer, N.; Sun, Y.; Fu, P.; Zhang, J.; Lin, Y.; Wang, X.; Shao, L.; Chen, J.; Zhang, X.; Wang, Z.; Wang, W., A conceptual framework for mixing structures in individual aerosol particles. *Journal of Geophysical Research: Atmospheres* **2016,** *121*, 13,784-13,798.

34. Wang, Q.; Huang, R. J.; Cao, J.; Han, Y.; Wang, G.; Li, G.; Wang, Y.; Dai, W.; Zhang, R.; Zhou, Y., Mixing State of Black Carbon Aerosol in a Heavily Polluted Urban Area of China: Implications for Light Absorption Enhancement. *Aerosol Science and Technology* **2014,** *48*, 689-697.

35. China, S.; Scarnato, B.; Owen, R. C.; Zhang, B.; Ampadu, M. T.; Kumar, S.; Dzepina, K.; Dziobak, M. P.; Fialho, P.; Perlinger, J. A.; Hueber, J.; Helmig, D.; Mazzoleni, L. R.; Mazzoleni, C., Morphology and mixing state of aged soot particles at a remote marine free troposphere site: Implications for optical properties. *Geophysical Research Letters* **2015,** *42*, 1243-1250.

36. Peckhaus, A.; Grass, S.; Treuel, L.; Zellner, R., Deliquescence and efflorescence behavior of ternary inorganic/organic/water aerosol particles. *The journal of physical chemistry. A* **2012,** *116*, 6199-6210.

37. Liu, L.; Mishchenko, M. I.; Patrick Arnott, W., A study of radiative properties of fractal soot aggregates using the superposition T-matrix method. *Journal of Quantitative Spectroscopy and Radiative Transfer* **2008,** *109*, 2656-2663.

38. Peng, J.; Hu, M.; Guo, S.; Du, Z.; Zheng, J.; Shang, D.; Levy Zamora, M.; Zeng, L.; Shao, M.; Wu, Y. S.; Zheng, J.; Wang, Y.; Glen, C. R.; Collins, D. R.; Molina, M. J.; Zhang, R., Markedly enhanced absorption and direct radiative forcing of black carbon under polluted urban environments. *Proceedings of the National Academy of Sciences of the United States of America* **2016,** *113*, 4266-4271.

39. Chakrabarty, R. K.; Beres, N. D.; Moosmüller, H.; China, S.; Mazzoleni, C.; Dubey, M. K.; Liu, L.; Mishchenko, M. I., Soot superaggregates from flaming wildfires and their direct radiative forcing. *Scientific Reports* **2014,** *4*, 5508, doi: 10.1038/srep05508.

40. Chakrabarty, R. K.; Moosmüller, H.; Garro, M. A.; Arnott, W. P.; Walker, J.; Susott, R. A.; Babbitt, R. E.; Wold, C. E.; Lincoln, E. N.; Hao, W. M., Emissions from the laboratory combustion of wildland fuels: Particle morphology and size. *Journal of Geophysical Research* **2006,** *111*, doi: 10.1029/2005jd006659.

41. Wentzel, M.; Gorzawski, H.; Naumann, K. H.; Saathoff, H.; Weinbruch, S., Transmission electron microscopical and aerosol dynamical characterization of soot aerosols. *Journal of Aerosol Science* **2003,** *34*, 1347-1370.

42. Chen, C.; Fan, X.; Shaltout, T.; Qiu, C.; Ma, Y.; Goldman, A.; Khalizov, A. F., An unexpected restructuring of combustion soot aggregates by subnanometer coatings of polycyclic aromatic hydrocarbons. *Geophysical Research Letters* **2016,** *43*, 11,080-11,088.

43. Bambha, R. P.; Dansson, M. A.; Schrader, P. E.; Michelsen, H. A., Effects of volatile coatings and coating removal mechanisms on the morphology of graphitic soot. *Carbon* **2013,** *61*, 80-96.

44. Wozniak, M.; Onofri, F. R. A.; Barbosa, S.; Yon, J.; Mroczka, J., Comparison of methods to

derive morphological parameters of multi-fractal samples of particle aggregates from TEM images. *Journal of Aerosol Science* **2012,** *47*, 12-26.

45. Leung, K. K.; Schnitzler, E. G.; Dastanpour, R.; Rogak, S. N.; Jäger, W.; Olfert, J. S., Relationship between Coating-Induced Soot Aggregate Restructuring and Primary Particle Number. *Environmental Science & Technology* **2017,** *51*, 8376-8383.

46. Leung, K. K.; Schnitzler, E. G.; Jäger, W.; Olfert, J. S., Relative Humidity Dependence of Soot Aggregate Restructuring Induced by Secondary Organic Aerosol: Effects of Water on Coating Viscosity and Surface Tension. *Environmental Science & Technology Letters* **2017,** *4*, 386-390.

47. Sorensen, C. M.; Chakrabarti, A., The sol to gel transition in irreversible particulate systems. *Soft Matter* **2011,** *7*, 2284-2296.

48. Torsten, T.; Zsófia, J.; Maria, M.; Roberto, C.; Martin, G.; Maarten, F. H.; Peter, F. D.; Berko, S.; André, S. H. P.; Ernest, W.; Urs, B., Changes of hygroscopicity and morphology during ageing of diesel soot. *Environmental Research Letters* **2011,** *6*, doi: 10.1088/1748-9326/6/3/034026.

49. Ma, X.; Zangmeister, C. D.; Gigault, J.; Mulholland, G. W.; Zachariah, M. R., Soot aggregate restructuring during water processing. *Journal of Aerosol Science* **2013,** *66*, 209-219.

50. Filippov, A. V.; Zurita, M.; Rosner, D. E., Fractal-like Aggregates: Relation between Morphology and Physical Properties. *Journal of colloid and interface science* **2000,** *229*, 261-273.

51. Wu, Y.; Cheng, T.; Zheng, L.; Chen, H., Optical properties of the semi-external mixture composed of sulfate particle and different quantities of soot aggregates. *Journal of Quantitative Spectroscopy and Radiative Transfer* **2016,** *179*, 139-148.

52. Smith, A. J. A.; Grainger, R. G., Simplifying the calculation of light scattering properties for black carbon fractal aggregates. *Atmospheric Chemistry and Physics* **2014,** *14*, 7825-7836.

53. Radney, J. G.; You, R.; Ma, X.; Conny, J. M.; Zachariah, M. R.; Hodges, J. T.; Zangmeister, C. D., Dependence of soot optical properties on particle morphology: measurements and model comparisons. *Environmental science & technology* **2014,** *48*, 3169-76.

54. He, C.; Takano, Y.; Liou, K.-N.; Yang, P.; Li, Q.; Mackowski, D. W., Intercomparison of the GOS approach, superposition T-matrix method, and laboratory measurements for black carbon optical properties during aging. *Journal of Quantitative Spectroscopy and Radiative Transfer* **2016,** *184*, 287-296.

Figure Captions

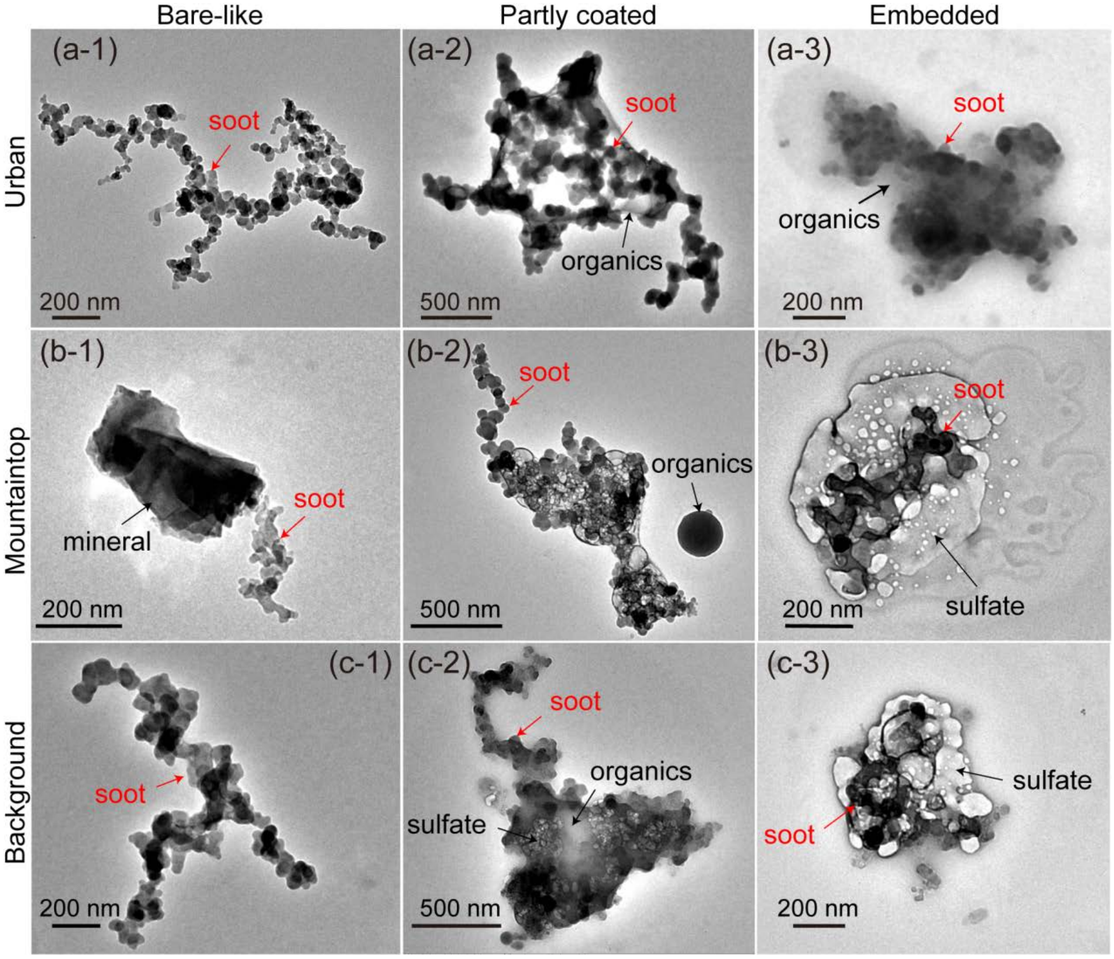

Figure 1. TEM images of individual soot particles collected at the urban site (a-1/2/3), the mountaintop site (b-1/2/3), and the background site (c-1/2/3). Soot particles are classified into three types: bare-like (a/b/c-1), partly coated (a/b/c-2), and embedded (a/b/c-3).

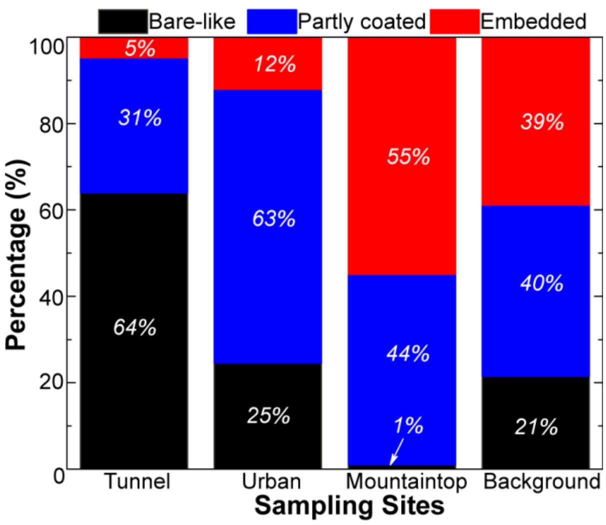

Figure 2. The percentages of bare-like, partly coated, and embedded soot particles collected at four sampling sites. 147, 216, 295, and 121 soot particles were analyzed in the samples collected at the tunnel, urban, mountaintop, and background sites, respectively.

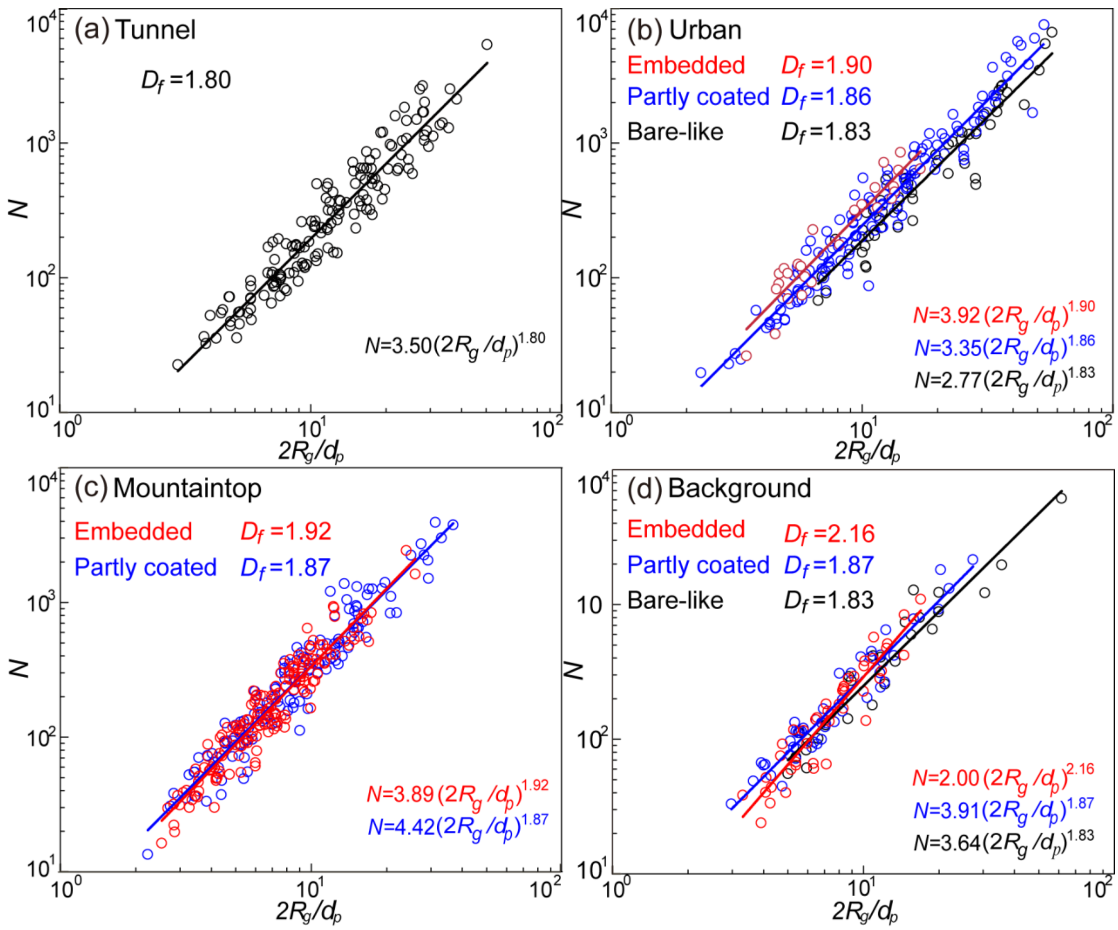

Figure 3. The fractal dimensions of different types of soot collected at the tunnel (a), urban (b), mountaintop (c), and background (b) site. For each site, the lines and circles represent bare-like (black), partly coated (blue), and embedded (red) soot particles.

For Table of Contents Use Only

Fractal Dimensions and Mixing Structures of Soot Particles during Atmospheric Processing

Yuanyuan Wang[1,2], Fengshan Liu[3], Cenlin He[4], Lei Bi[2], Tianhai Cheng[5], Zhili Wang[6], Hua Zhang[7,8], Xiaoye Zhang[6], Zongbo Shi[9], Weijun Li[*2]

[1]Environment Research Institute, Shandong University, Jinan, Shandong 250100, China

[2]Department of Atmospheric Sciences, School of Earth Sciences, Zhejiang University, Hangzhou, 310027, China

[3]Measurement Science and Standards, National Research Council, Ottawa, Ontario K1A 0R6, Canada

[4]Department of Atmospheric and Oceanic Sciences and Joint Institute for Earth System Science and Engineering, University of California, Los Angeles, CA90095, USA

[5]State Key Laboratory of Remote Sensing Science, Institute of Remote Sensing and Digital Earth, Chinese Academy of Sciences, Beijing, 100101, China

[6]Chinese Academy of Meteorological Sciences, Beijing 100081, China

[7]Collaborative Innovation Center on Forecast and Evaluation of Meteorological Disasters, Nanjing University of Information Science & Technology, Nanjing 210044, China

[8]Laboratory for Climate Studies, National Climate Center, China Meteorological Administration, Beijing 100081, China

[9]School of Geography, Earth and Environmental Sciences, University of Birmingham, Birmingham B15 2TT, U.K